Discrete Element Modeling of shielding and size effects during single particle crushing

Pei Wang, Chloé Arson*

School of Civil and Environmental Engineering at the Georgia Institute of Technology, 790 Atlantic Drive, Atlanta, GA 30332-0355

Abstract

In granular assemblies such as soil, ballast, cementitious aggregates, food and medical products, particle fragmentation and crushing alter material properties. The goal of this research work is to better understand the microstructure parameters that control the triggering of fragmentation, and to predict how microstructure evolution consequent to crushing can actually enhance or reduce material properties. We focused on size and shielding effects, which respectively refer to the decrease of particle strength with increasing particle size, and to the increase of particle strength with the redistribution of stress towards hydrostatic stress conditions upon crushing of neighboring particles. We calibrated the parameters of a Distinct Element Method (DEM) cluster model of crushable particle so as to match the displacement and axial force obtained experimentally at the first particle fragmentation. In order to study the influence of the coordination number on particle crushing, we modeled the mechanical confinement effect of neighboring particles by placing rigid

*School of Civil and Environmental Engineering at the Georgia Institute of Technology, 790 Atlantic Drive, Atlanta, GA 30332-0355

Email address: chloe.arson@ce.gatech.edu (Chloé Arson)

walls around the DEM cluster. In order to understand why larger particles have lower tensile strength, we studied size effects on the crushing process of clusters with and without internal flaws. We found that for clusters with a porosity ranging between 0% and 30%, tensile strength only depends on porosity and not on flaw size. Overall results show that particle strength depends: (1) linearly on particle coordination number; (2) quadratically on particle porosity. Theoretical and DEM modeling of particle crushing will advance the fundamental understanding of energy transfer in particulate media.
Keywords: particle crushing, shielding effect, size effect, DEM

---

1. Introduction

Mechanical particle crushing is a problem that is omnipresent in civil engineering and in the mineral industry [1][2][3]. The crushing of a granular assembly can be described by a sequence of elementary events during which a single particle breaks into several fragments under the influence of compressive stresses. In the laboratory, single particle crushing tests are conducted by applying a uniaxial compression force with two horizontal platens [4][5]. The strength of a granular assembly and the force necessary to break a given percentage of elementary particles (e.g. sand grains, rock stones) both depend on material properties, particles' size and shape, as well as the coordination number. The coordination number of a particle is defined as the number of grains that are in contact with that particle (and potentially, applying a reaction force on that particle).

A high coordination number is known to prevent crushing. The mechanism can be explained by the redistribution of concentrated compression forces at particle contacts into a distributed pressure that is close to hydrostatic conditions. Hence the induced tensile stress developed inside the grain is reduced. A few analytical models were proposed to understand this phenomenon, known as "shielding effect". Jaeger [6] derived the expression of stress in the section of a cylinder subjected to four compressive line loads positioned 45^o apart from each other in the section. The analytical solution shows that the maximum tensile stress and the corresponding breakage force are less than in the case of a cylinder loaded with only two line loads positioned 90^o apart. Tsoungui modeled contact forces applied to a particle by calculating four equivalent contact forces in two principal directions, and expressed the principal stresses and maximum tensile stresses in the particle [7]. The tensile stress was compared to the particle strength to predict fracture propagation and crushing at the particle scale. Unfortunately the solution was only provided for 2D problems and the calculation method assumes that the particle cannot break if the two principal stresses are equal, which is not practical for sand or rock particles. In studies based on the Distinct Element Method (DEM), the influence of the number of contacts between crushable particles, modeled as clusters of bonded elementary particles ("balls"), was not examined. Instead, authors focused on the number of contacts (or bonds) of the elementary balls making the cluster [8][9]. Therefore, the influence of the coordination number on particle crushing is still not fully understood.

Statistically, the largest particles in a granular assembly have the highest

coordination number. Therefore, according to the shielding effects, the probability of breakage of a particle should decrease as the relative size of that particle (i.e. the actual particle size divided by the average particle size in the assembly) increases. However the probability of breakage of a particle also depends on the size of that particle, regardless of the coordination number. This size effect was noted in strength test experiments performed in concrete structures, rock samples and granular materials [10][11][12]. If one accepts that larger particles tend to have larger internal flaws than smaller particles, then it is possible to explain, based on the Griffith's theory, why particle strength decreases as particle size increases [13][14]. Several empirical equations were obtained from single-particle uniaxial compression tests, in order to relate particle strength to particle size. For instance, Hiramatsu [15] studied the stress distribution in a single particle subjected to a concentrated load by means of photo-elastic experiments and mathematical analysis. In order to predict the strength of real rock particles, a fitting parameter (κ) was introduced in the analytical expression of stress in a spherical particle:

$$\sigma_f = \frac{\kappa F_f}{d^2}, \tag{1}$$

where σ_f is the tensile stress at failure, F_f is the corresponding compressive force applied and d is a characteristic particle dimension. The value of κ was fitted to experimental results obtained during compression tests. Several values were reported: $\kappa = 0.9$ in [15]; $\kappa = 0.58$ and $\kappa = 0.82$ in [5]. Based on single-particle compression tests, Lee [16] proposed the following relationship between particle strength and particle size:

$$\sigma_f = K d^b. \tag{2}$$

The size effect parameter b, which is the slope of the force-size curve in logarithmic coordinates, is typically a negative number, in the order of -1 to -0.1. Equations 1 and 2 suggest that the peak force F_f is proportional to an exponent of the particle size (d^{α}). This hypothesis was verified by another empirical study [10], which showed that for α smaller than 2.0, tensile strength decreases when particle size increases.

The Weibull theory can be used to predict the probability of failure of a particle that contains flaws of various sizes, or the probability of survival (i.e. the probability of non crushing) of a particle of a given size inside a granular assembly [17][18]. At the scale of a Representative Elementary Volume (REV) of granular material, Weibull models can be verified by plotting the particle size distribution at several key stages of a uniaxial compression test [19][20]. At the particle scale, the Weibull theory was used to predict the breakage force for clusters of various sizes, made of bonded particles and internal flaws [8]. However the porosity of the clusters was not provided, which makes it impossible to explain size effects, because the influence of the flaw size cannot be distinguished from that of the number of flaws or that of the flaw volumetric fraction. Weibull models can be fitted to predict force-displacement curves and particle size distributions observed during compression tests performed in the laboratory or simulated with the DEM. However, there is still a lack of understanding of what originates size effects, and how size effects counter-act shielding effects in the process of crushing.

In this paper, we analyze separately shielding and size effects with a

DEM model of single-particle crushing designed with PFC3D 4.0. We calibrate our cluster model against published force-displacement curves obtained during sand particle crushing tests. The strength predicted by the model is verified by applying the Buckingham Π theorem (Section 2). We simulate axial compression after applying several reaction forces around the cluster, and express a relationship between the breakage force and the coordination number (Section 3). Lastly, we simulate single particle crushing with various cluster sizes, cluster porosities, flaw sizes and number of flaws (Section 4).

2. DEM Model of Crushable Particle

2.1. Constitutive Model used in the Particle Flow Code (PFC3D)

In the following, we represent a crushable particle as a spherical cluster of bonded, hexagonally packed, equally sized, non-breakable spheres ("balls"). Cluster crushing is modeled as bond breakage. The simulations are conducted with PFC3D, a DEM program introduced by Cundall and Strack [21] and then further developed by Itasca [22]. In PFC3D, rigid "balls" and rigid "walls" are allowed to overlap over a contact area of negligible size compared to that of the balls. Balls can be bonded together to form clusters of different sizes and shapes. Interactions between bonded balls are governed simultaneously by three constitutive laws: a ball contact-stiffness model, a ball slip model and a bond model. Once the tensile strength or shear strength of a bond is reached during loading, the bond breaks and is deleted from the cluster model.

We use a linear contact-stiffness model, in which the relationship between

the force and the relative displacement at the $i-th$ ball contact is expressed as:

$$F_i^n = k^n U^n n_i, \ \Delta F_i^s = -k^s \Delta U_i^s \tag{3}$$

where F_i^n and ΔF_i^s are respectively the normal contact force and shear force-increment; k^n and k^s are respectively the normal stiffness and the shear stiffness at the contact; U^n is the normal overlap between the two balls in contact; n_i is the unit vector along the line that links the two ball centers; and U_i^s is the shear component of the increment of contact displacement. Note that the linear contact-stiffness model assumes that the normal and shear stiffnesses of the contact do not depend on the displacement vector.

In the slip model used in the simulations, the maximum shear force at a contact is expressed as:

$$F_{max}^s = \mu |F_i^n| \tag{4}$$

If $|F_i^s| > F_{max}^s$, then slip occurs and the magnitude of F_i^s is set to F_{max}^s.

We use the parallel bond model, in which bonds between balls are represented as short beams of circular cross-section ("disks"). Parallel bonds transmit both forces ($\bar{F}_i$) and moments ($\bar{M}_i$), which are split into a component normal to the contact plane ($\bar{F}_i^n$, $\bar{M}_i^n$) and a shear component contained in the contact plane ($\bar{F}_i^s$, $\bar{M}_i^s$), as follows:

$$\bar{F}_i = \bar{F}_i^n + \bar{F}_i^s, \quad \bar{M}_i = \bar{M}_i^n + \bar{M}_i^s \tag{5}$$

Initially when a bond is created with PFC3D, internal bond forces and moments are set to zero. During a loading increment, the relative displacement

and rotation between the two bonded balls generate an increment of force and moment. The elastic increments of force and moment are calculated as follows:

$$\Delta\bar{F}_i^n = (-\bar{k}^n A\Delta U^n)n_i,\ \Delta\bar{F}_i^s = -\bar{k}^s A\Delta U_i^s \tag{6}$$

$$\Delta\bar{M}_i^n = (-\bar{k}^s J\Delta\theta^n)n_i,\ \Delta\bar{M}_i^s = -\bar{k}^n I\Delta\theta_i^s \tag{7}$$

In which θ^n and θ_i^s are the bond incremental angles and A is the area of the disk that forms the cross section area of the bond ($A = \pi\bar{R}^2$). J and I are the polar moments of inertia, calculated by $J = \frac{1}{2}\pi\bar{R}^4$ and $I = \frac{1}{4}\pi\bar{R}^4$ respectively. The bond model depends on five parameters: the normal and shear stiffnesses ($\bar{k}^n$ and $\bar{k}^s$); the normal and shear strengths ($\bar{\sigma}_c$ and $\bar{\tau}_c$); and the radius of the bond cross section ($\bar{R}$). If the maximum tensile or shear stress exceed the corresponding strength, then the parallel bond breaks and is deleted from the DEM model.

2.2. Model Calibration: Single particle crushing simulation

In the following, we calibrate the five bond parameters of the DEM cluster model to match force-displacement curves obtained experimentally during single-particle crushing tests performed on sand [23]. In order to reproduce the conditions of the experiment, the diameter of the cluster was set to 0.729mm (which is the diameter of the sand grains). In order to minimize the rotation of the cluster and the yielding of asperities before the first fragmentation [4][24], we deleted a few layers of rigid balls at the top and bottom of the cluster. The diameter of the cluster was reduced by 5% in the axial direction, and maintained as such in the lateral direction. The model contained 11,000 rigid balls, which allowed considering the cluster as a REV [8]. We

arranged the rigid balls into a Hexagonal Close Packing (HCP) in order to maximize the density of the cluster and the number of contacts between the balls, and therefore get a representative model of crushable particle without flaws, as advocated in previous studies conducted with PFC3D [23][25][26]. The loading platens were modeled by disk-shaped rigid walls (e.g., [27]). The diameter of the disk walls was equal to that of the cluster. In order to model the platens as rigid bodies, the stiffness of the walls was set to 1×10^{30}N/m, i.e. several orders of magnitude higher than the stiffness of the balls and of the bonds.

The cluster was subjected to gravity forces before being compressed axially. During the loading phase, the top and bottom walls were subjected to a constant velocity, which was chosen small enough to simulate a quasi-static loading (note that the breakage force depends on the loading velocity otherwise). The DEM algorithm is stable only if the time step chosen for the loading increments is smaller than a critical value, which depends the mass and stiffness of each ball and is of the order of 10^{-7} to $10^{-9}\,s$ for soils and rocks [22]. Loading velocities ranging from 0.2 to 1.28m/s were used in [26][28][29]; these high loading increments were chosen to ensure algorithm stability while reducing the simulation time. By contrast, we used differential density scaling in order to apply a low wall velocity with a reduced number of load steps: the time step was set to unity and the inertial mass of each ball was adapted at the beginning of each load step. The loading rate applied in the simulations presented in the following was 5×10^{-7}mm/s (which represents quasi-static loading conditions). During the entire simulation, we

monitored the intensity of the contact forces at the walls, the displacements of the walls and the number of broken bonds. The five DEM bond parameters were fit to match the force intensity and wall displacement obtained experimentally at the first peak of the force-displacement curve (i.e., at the first fragmentation). The calibrated parameters are listed in Table 1.

Table 1: Parameters used in DEM simulations

Diameter of sphere (R): mm	1.4×10^{-2}
Density of sphere (ρ): kg/m^3	3581
Normal and shear stiffness of each sphere (k^n and k^s): N/m	1×10^5
Normal and shear bond strength (σ_c and τ_c): MPa	130
Normal and shear stiffness of parallel bond ($\bar{k}^n$ and $\bar{k}^s$): N/m^3	1.6×10^{13}
Frictional coefficient of sphere (μ)	0.5

The HCP of rigid balls has symmetries. In order to assess the potential anisotropy induced by the HCP orientation on cluster mechanical properties, we compared the results obtained with the set of DEM bond parameters reported in Table 1 for the following HCP orientations (in reference to the horizontal): 0°(horizontal), 30°, 45°, 60° and 90°(vertical). The test set up for HCPs oriented by an angle of 0° and 45° to the horizontal are shown in Figure 1. Figure 2 shows the force-displacement curves obtained during the simulations. All HCP orientations exhibit similar trends. After the first fragmentation, internal forces in the cluster are relaxed, which explains the

sudden drop of force after the peak. At larger orientation angles (i.e., when the HCP orientation deviates from the horizontal), the breakage plane is more likely to be parallel to the HCP layers. For an angle of 0° (i.e, horizontal HCP), the breakage plane is vertical (i.e. perpendicular to the lattice), which is similar to what is observed in Brazilian tests performed on rock samples. It is noteworthy that for the vertical HCP, a force drop occurred before the first fragmentation (point A in Figure 2). According to the video generated during the simulation, this drop, although small, actually corresponded to a rotation of the cluster and the yielding of some asperities. The particle broke after rotation, when the axis of the loading was alined with a plane of weakness of the cluster. To avoid rotation, we present results obtained with the horizontal HCP model, which is used in all the following simulations for consistency.

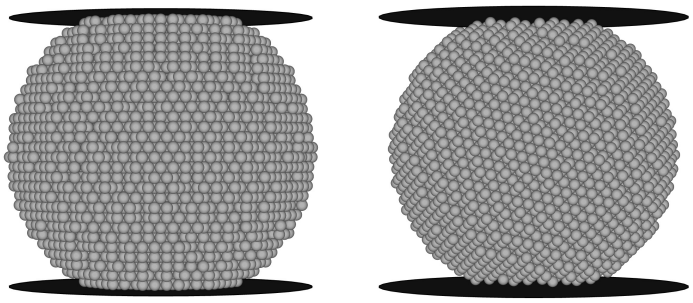

Figure 1: Cluster formed by bonded non-breakable spheres arranged into a Hexagonal Close Packing (HCP). a. HCP orientation of 0° to the horizontal plane ("Horizontal HCP"). b. HCP orientation of 45° to the horizontal plane.

Note that since the balls and bonds obey a linear elastic behavior before

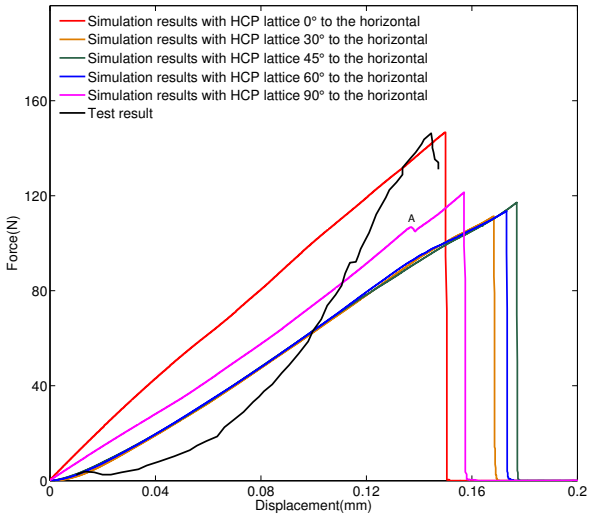

Figure 2: Force-displacement curves during a uniaxial compression test simulated up to the first fragmentation: calibration of the DEM cluster model against experimental test results, with various HCP orientations (in reference to the horizontal plane).

breakage, the force-displacement curve is linear before the first peak. In the experiment, the curve is non-linear due to the presence of heterogeneities in the particle and due to the expansion of contact areas during compression, which increases particle stiffness. Typical simulation results are shown in Figure 3, in which we can see that due to the symmetry imposed to the model, the particle breaks along the loading axis. When the first peak force is reached, the cluster breaks into four main pieces and a number of smaller fragments, which is in agreement with experimental observations [23].

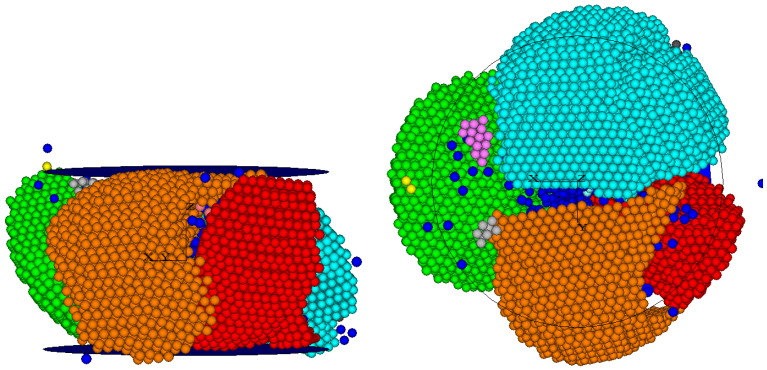

Figure 3: Lateral view (left) and top view (right) of the cluster after the first fragmentation (horizontal HCP).

2.3. Model validation using the Buckingham Π *theorem*

According to the Buckingham Π theorem, physical laws should not depend on the units of measurement [30]. Huang [31] suggested that for a DEM model that contains bonded balls, the set of micro-parameters that control macro-properties is $\{k_n, k_s, T_n, T_s, \mu, R, n, \rho, L, V\}$, where T_n and T_s

are respectively the normal and shear strengths of the contact bonds, R is the average ball size, n is the porosity, ρ is the mass density of the elementary balls, L is the sample size and V is the loading speed. The failure of the specimen is governed by the following dimensionless parameters: $\{k_nR/T_n, T_n/T_s, \mu, k_s/k_n, n, R/L, V/\sqrt{k_n/\rho}\}$. In the present case, the ratio $V/\sqrt{k_n/\rho}$ can be ignored because the loading is quasi-static. In order to simplify the analyses with the parallel bond model, we replace the contact bond strengths T_n and T_s (defined in force) by the strengths σ_c and τ_c (defined in stress). After introducing the normal and shear parallel bond stiffnesses $\bar{k}^n$ and $\bar{k}^s$, two dimensionless parameters are added to the list of controlling variables: the ratio of parallel bond normal stiffness and parallel bond shear stiffness $\bar{k}^n/\bar{k}^s$, and the ratio of parallel bond stiffness and ball stiffness $\bar{k}^nR^2/k_n$. Other studies indicate that the ball size also needs to be considered because it has effects on the behavior of particulate assemblies in PFC simulations [32][33][34]. Accordingly, we propose to express the relationship between micro-parameters and sample tensile strength (σ_t) as:

$$\sigma_t = \sigma_c\Phi(\frac{k_n}{\sigma_cR}, \frac{\sigma_c}{\tau_c}, \mu, \frac{k_n}{k_s}, \frac{L}{R}, \frac{\bar{k}^nR^2}{k_n}, \frac{\bar{k}^n}{\bar{k}^s}) \tag{8}$$

We simulated a uniaxial compression for several cluster sizes. The ball size R, the contact normal stiffness k_n and the parallel bond stiffnesses $\bar{k}^n$ and $\bar{k}^s$ were adjusted in order to maintain all the dimensionless DEM parameters constant. We observe that the breakage force increases according to a power law (Figure 4) but that the strength of the cluster remains fairly constant (Figure 5). The result are in agreement with the Buckingham Π theorem, which states that under constant DEM non-dimensional parameters, the cluster strength should be the same for all cluster sizes tested (Equation

8).

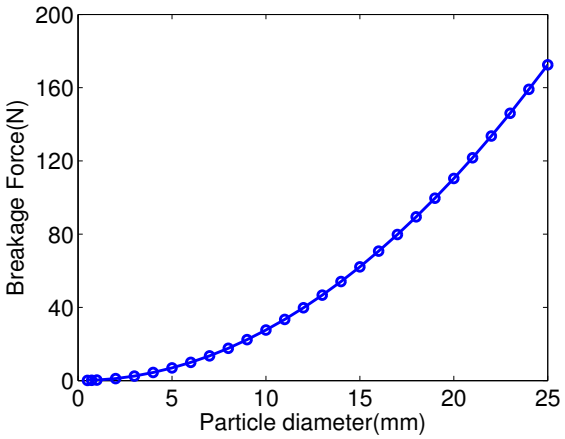

Figure 4: Validation of the cluster model with the Π theorem: variations of the breakage force with the cluster size.

3. Modeling of the Shielding Effect

We now use the calibrated cluster model presented in Section 2 to simulate shielding effects at the particle scale. Particles neighboring the cluster are represented by walls that produce a reaction force at the boundaries of the cluster. This modeling strategy allows uncoupling the variation of the coordination number from the rearrangement of the fabric that is expected to occur during crushing. Statistically, the coordination number in a granular material increases when the contrast in size between particles is large. The surface area (which determines the maximum coordination number) is proportional to d^2 (in which d is the diameter of the particle). In well-graded sands and rocks which contain both fine- and coarse-grained soils, the value

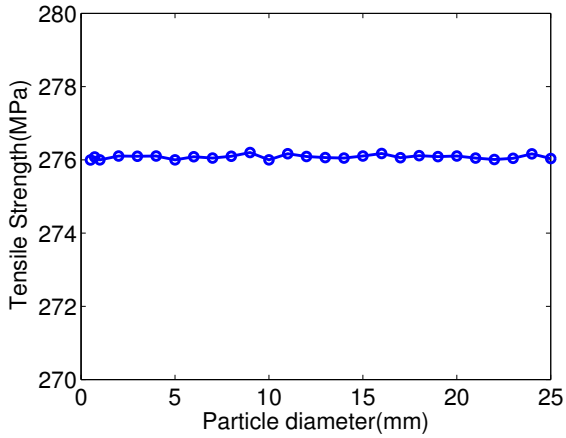

Figure 5: Validation of the cluster model with the Π theorem: variations of the cluster strength with the cluster size.

of d_{max}/d_{min} often exceeds 10 [35], which implies a difference of surface area of two orders of magnitude and therefore, high coordination numbers. A broad range of coordination numbers (i.e., up to 120) is explored in order to check whether shielding effects can be explained by a redistribution of contact forces from a set of punctual loads (applied over a limited number of neighboring grains) to a quasi-hydrostatic stress (applied through a high number of contacts). The cluster is axially loaded by the top and bottom walls (called the loading walls in the following), and confined by passive walls (called shielding walls in the following). We vary the number of shielding walls in order to establish a relationship between the coordination number of a particle and the axial force needed to trigger the first fragmentation.

3.1. Construction of the DEM shielding model

The shielding model was obtained in four steps, as shown in Figure 6:

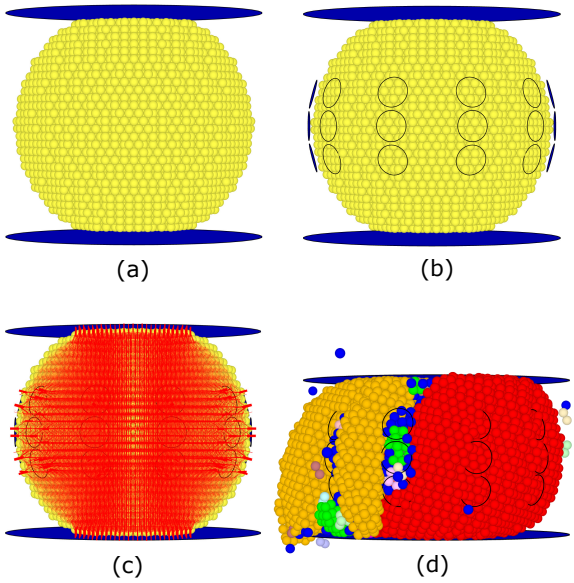

Figure 6: Steps to generate a shielding model in DEM. (a) Generate the cluster and loading walls. (b) Generate the shielding walls. (c) Generate the reaction forces at the shielding walls. (d) Crush the cluster.

1. Generate the cluster and the loading walls. This step was similar to that used for the simulations presented in Section 2 for calibration.
2. Generate the shielding walls. Shielding walls were modeled as small disk walls that are tangent to the cluster. The radius of the shielding walls was 0.05mm (about 3 times the radius of the non-breakable balls inside the cluster), which ensures that the shielding walls produce a confinement without punching the cluster. During the crushing process, shielding walls redistributed contact forces, which reduced concentrated compressive forces at the contacts and tensile stress in the cluster. For low coordination numbers (below 60), random wall distributions resulted in highly heterogeneous contact distributions on the cluster. Stress redistribution resulted in stress concentrations instead of the expected hydrostatic stress. Therefore, for a coordination number up to 60, shielding walls were positioned according to a symmetric distribution. Above 60, both symmetric and random wall distributions were investigated. The procedure adopted to generate symmetric wall distributions is explained in Figure 7 and Table 2. Random wall distributions were generated by random point picking, with normal vectors pointing towards the origin [36], as shown in Figure 8. An algorithm was written to delete overlapping shielding walls. Gravity forces were applied after all walls were created.
3. Generate reaction forces at the shielding walls. The shielding walls were displaced towards the center of the cluster under controlled velocity in order to ensure contact with the cluster. The velocity was set to 5×10^{-7}mm/s (same velocity as that used for calibration), until the

first bond breakage occurred in the cluster. Since the total number of bonds exceeded 60,000, the effect of a single bond breakage on the fragmentation of the whole cluster was ignored. After the first bond breakage, the velocity of the shielding walls was set to zero.

4. Crush the cluster. The two loading walls were displaced at a velocity of 5×10^{-7}mm/s, while keeping the shielding walls at a fixed position. Reaction forces generated in the loading walls were monitored.

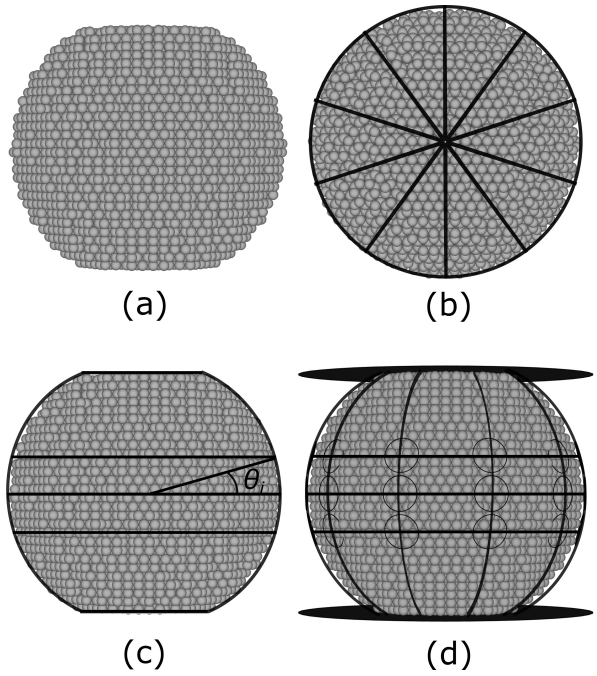

Figure 7: Procedure to generate a model with symmetric distribution of 30 shielding walls (10×3): (a) generate the HCP cluster; (b) divide the cluster into ten longitudinal slices (top view); (c) find circles at a longitude θ_i (in reference to the horizontal) at the surface of the particle (side view); (d) generate walls at the intersection of the circles with the longitudinal lines (side view).

Table 2: Geometric parameters of the symmetric distribution of shielding walls. The number of walls $N = N_1 \times N_2$ is the product of the number of wall centroids in a plane (N_1) by the number of horizontal planes containing wall centroids (N_2). θ_i is the orientation of the wall centroids in reference to the horizontal.

Wall numbers	θ_i	Wall numbers	θ_i
$4 \times 1 = 4$	0	$8 \times 5 = 40$	$0, 15, 30$
$8 \times 1 = 8$	0	$15 \times 3 = 45$	$0, 15$
$10 \times 1 = 10$	0	$10 \times 5 = 50$	$0, 15, 30$
$12 \times 1 = 12$	0	$8 \times 7 = 56$	$0, 15, 30, 45$
$15 \times 1 = 15$	0	$12 \times 5 = 60$	$0, 15, 30$
$6 \times 3 = 18$	0,15	$10 \times 7 = 70$	$0, 15, 30, 45$
$8 \times 3 = 24$	0,15	$15 \times 5 = 75$	$0, 15, 30$
$10 \times 3 = 30$	0,15	$12 \times 7 = 84$	$0, 15, 30, 45$
$12 \times 3 = 36$	0,15	$15 \times 7 = 105$	$0, 15, 30, 45$

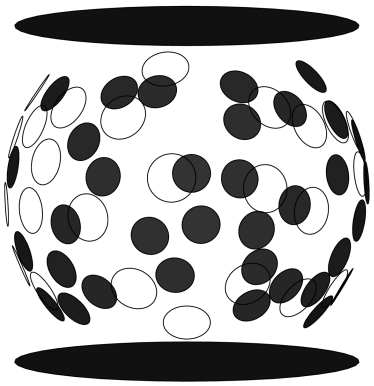

Figure 8: Random distribution of 60 shielding walls, generated by random point picking. An algorithm was written to avoid overlap between the shielding walls.

3.2. Simulation Results

Figure 9 shows selected force-displacement curves obtained during the simulations. It is clear that the magnitudes of the peak force and of the wall displacements at the first fragmentation both increase with the number of shielding walls. For samples with high coordination numbers, we observed that particle fragments were all confined within the volume delimited by the shielding walls during the crushing. Therefore contact was maintained between the cluster and the loading walls, which explains why the magnitude of the force drop was smaller for a higher number of contact walls. Figure 10 shows the evolution of the number of broken bonds with the loading displacement. The sudden force drop observed for low coordination numbers in Figure 9 translates into a very sharp increase of the number of broken bonds - as opposed to the more gradual bond breakage evolution noted for higher coordination numbers. Overall, the steady increase of peak force with the coordination number illustrates the occurrence of shielding effects for both symmetric and random distributions of walls. Figure 11 shows that the peak force reached at the first cluster fragmentation is approximately proportional to the number of shielding walls. A linear regression provided a slope of 1.31 for both symmetric and random wall distributions. This linear relationship can be used to optimize the size distribution and packing (thus coordination number) of crushable particles inside a granular assembly to avoid crushing under quasi-static axial loading.

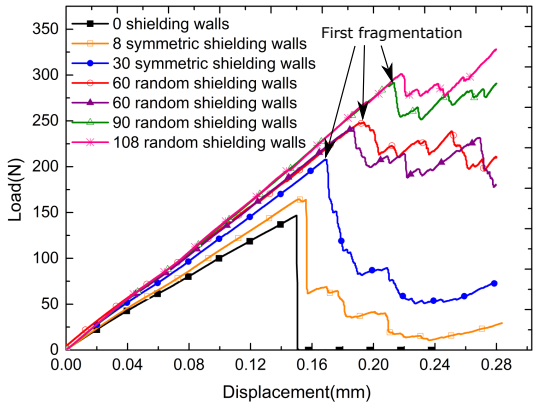

Figure 9: Force-displacement curve obtained with the shielding models.

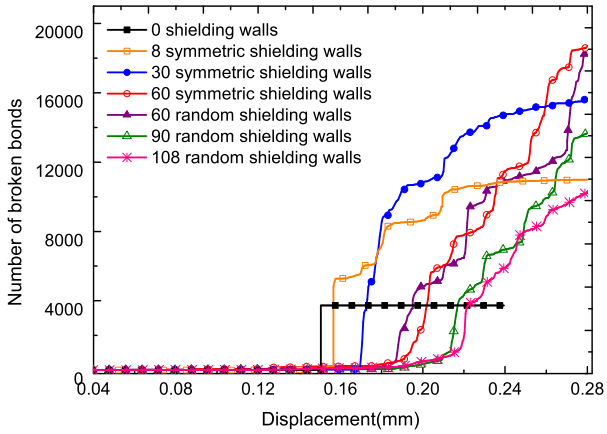

Figure 10: Evolution of the number of broken bonds with the cumulated displacement of the loading walls in the shielding models.

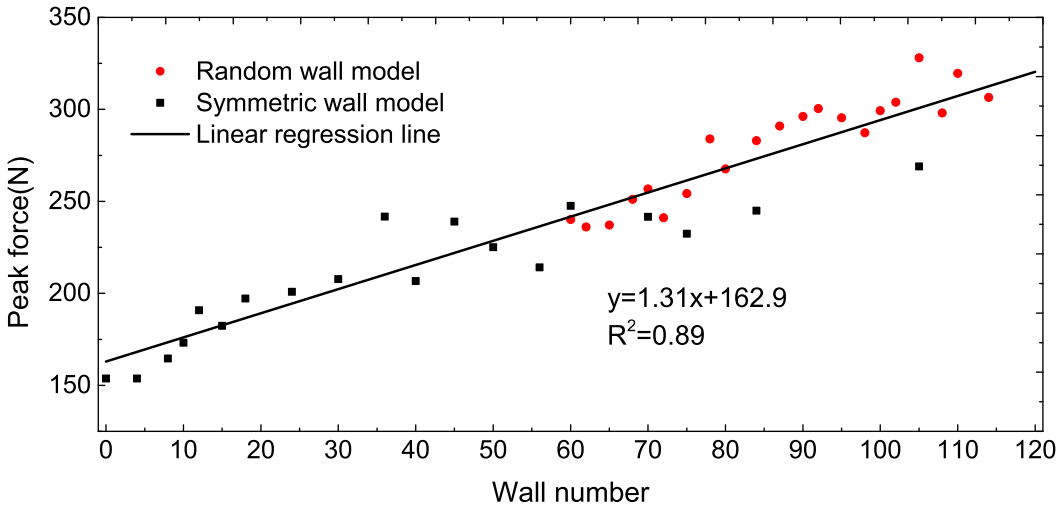

Figure 11: Relationship between the peak force reached at the first fragmentation and the number of shielding walls used in the simulations (coordination number of the cluster).

4. Modeling of the Size Effect

Numerous single-particle crushing experiments show that tensile strength increases when particle size decreases, which, according to previous studies, can be explained by the fact that smaller particles have less and smaller defects than larger particles [18]. The particle size exponent b in Equation 2 was found to be equal to -0.375, -0.343 and -0.420 for Leighton Buzzard sand, oolitic limestone and carboniferous limestone respectively [16]. In other materials, b was found to range between -0.7 and -0.3 [37, 38]. The micro-mechanical origin of size effects is still not fully understood. In the following, we explore several possible causes of size effects, including the particle size (with and without internal flaws), the flaw size, the number of flaws and the overall porosity of the crushable particle.

4.1. Effect of the cluster size, with and without internal flaws

We construct cluster models of various sizes, with the same elementary ball size and DEM parameters as those presented in Section 2. For each cluster size, we compare the results of uniaxial compression tests obtained with clusters that have 0% porosity (no internal flaw; solid volume fraction of about 74%, i.e. maximum packing density) with those obtained with clusters that have 10% porosity (i.e. with internal flaws). Porosity was created by removing randomly 10% of the elementary balls forming the cluster. Clusters had a diameter ranging from 0.1mm (34 elementary balls) to 1.9mm (230,000 balls).

Figure 12 shows that the peak force at first fragmentation varies with the diameter of the cluster (representing the crushable particle) according to a power law. The exponent is 1.96 for 0% porosity and 1.86 for 10% porosity. According to Equation 2, this implies that the tensile strength is proportional to $d^{-0.04}$ (respectively $d^{-0.14}$) for 0% porosity (respectively 10% porosity), i.e. that the tensile strength is almost constant (respectively slightly decreases as the size of the particle increases) for 0% porosity (respectively for 10% porosity). This statement is confirmed by the results presented in Figure 13. For instance, for 0% porosity, the tensile strength varies between 250MPa and 290MPa for cluster sizes varying from 0.2 to 1.9mm respectively (i.e. the slope of strength/size curve amounts to less than 15% of the magnitude of the tensile strength). Strength decreases with particle size for 10% porosity, which may be due to the higher number of voids at the contact between the particle and the platen, which increases the probability to initiate

cracks in the contact zone. Since flaws were randomly distributed to create a 10% porosity, the average number of contacts between balls was uniformly decreased, which generated higher stress concentrations, and therefore, reduced the strength of the cluster. We note that in relation 2, the absolute value of the exponent b that we obtain in our simulations is much smaller than that measured in the laboratory, which confirms that particle size does not control particle strength.

We also note that the tensile strength converges to a constant value for clusters 1mm in size and above, i.e. for clusters that contain at least 37,000 elementary balls (which corresponds to a ratio ball size/cluster size smaller than 0.014). We claim that below a ratio ball size/cluster size of 0.014, the cluster has an insufficient number of elementary balls to be considered as a REV. The results presented in Figure 13 indicate that for a fixed number of flaws (either zero flaw or a number of flaws equal to 10% of the elementary balls forming the cluster) and for a fixed flaw size (either null size or a size equal to the elementary ball size), size effects cannot be attributed to the size of the crushable particle.

4.2. Effect of the flaw size

According to Griffith theory, the strength of the crushable particle depends on the size of the largest flaw in that particle. In order to verify this statement, we simulated uniaxial compression tests with clusters that contained flaws. The simulations were performed with the cluster model calibrated in Section 2.2 with $N_1 = 653$, $N_2 = 1306$ and $N_3 = 1960$ flaws. In each simulation, flaws were equally sized. In each of the three cases under

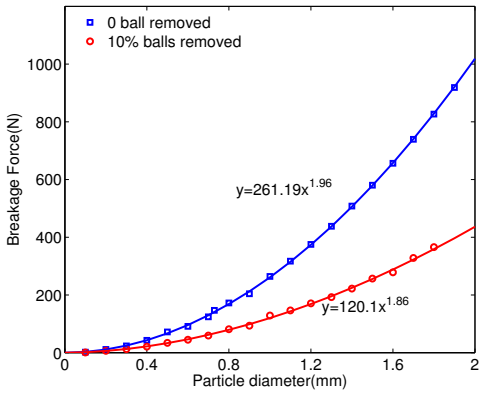

Figure 12: Relationship between the breakage force and the crushable particle size (fixed flaw size).

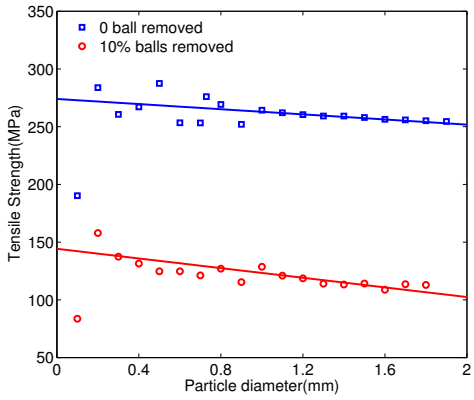

Figure 13: Relationship between the strength and the crushable particle size (fixed flaw size).

study (N_1, N_2 and N_3), we tested three uniform flaw size distributions, by deleting one, two or three elementary balls per flaw. We repeated the nine simulations several times and checked that similar results were obtained. We compared the results obtained with the same number of flaws but different flaw sizes, and we compared the results obtained with the same flaw size but different numbers of flaws. Results are shown in Figure 14. We verify that strength decreases when porosity increases, and we note that particle tensile strength decreases linearly with the flaw size. For the range of porosities and numbers of flaws investigated in this parametric study, it was not possible to simulate crushing for a large range of flaw sizes. We present results obtained for a larger span of flaw sizes in the next subsection.

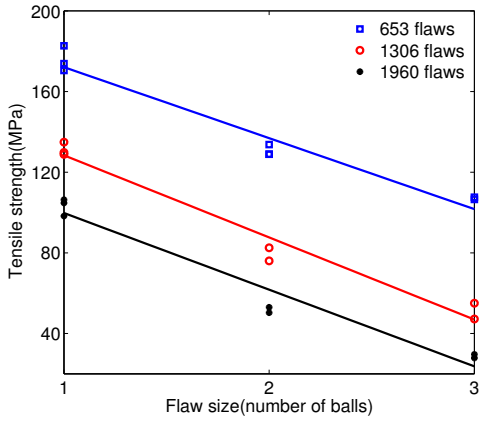

Figure 14: Effect of flaw size on particle tensile strength. Flaws were created by deleting elementary balls that formed the cluster. Three flaw sizes were studied, by deleting sets of three balls in contact, two balls in contact, or balls initially not in contact.

4.3. Effect of the number of flaws

In the following, we investigate the strength of particles that contain a variable number of equally sized flaws. The size and DEM parameters of the cluster are those presented in Section 2.2. Flaw sizes ranged between $n = 1$ to $n = 100$ times the elementary ball size. We started by generating a random distribution of flaw centroids. Then we deleted elementary balls containing the centroids ("centroid balls"). For $n \leq 10$, we created flaws by deleting $(n - 1)$ balls in contact with each centroid ball. For $n > 10$, we deleted all the elementary balls contained in a spherical control volume around the centroid balls. The size of the control volume was increased until it contained the desired number of elementary balls to be deleted. For the same level of porosity, the distribution of flaws was more uniform for smaller (and more numerous) flaws than for larger flaws. This explains why simulations were more difficult to reproduce when $n > 10$ than when $n \leq 10$. The results are presented in Figure 15. For each flaw size investigated, a linear relationship was found between the particle tensile strength and the logarithm of the number of flaws. We note that the slope is similar in all the simulations performed with $n \leq 10$. For larger flaws, the strength decreases at a faster rate with the number of flaws present in the cluster.

4.4. Effect of porosity

The previous parametric studies indicate that the size effects noted in particle strength are more likely attributed to the size and number of flaws, rather than to the size of the particle itself. In a crushable particle that contains equally sized flaws, are size effects due to the average flaw size or to the number of flaws? In order to answer this question, we compared the

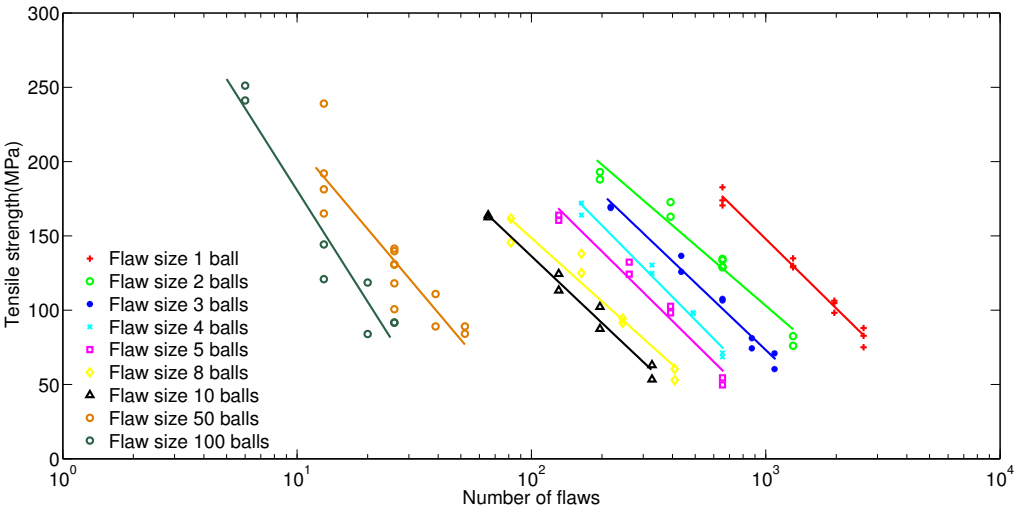

Figure 15: Effect of the number of flaws on particle tensile strength. Flaws were created by deleting elementary balls that formed the cluster. Groups of up to 100 balls in contact were deleted to produce flaws of different sizes.

results obtained for clusters of same porosity but different flaw size. Figure 16 shows the variations of particle strength with porosity (which was calculated as the percentage of elementary balls deleted to create particle flaws). We note that for a given particle porosity, particle strength decreases when porosity increases and does not vary with the flaw size. Laboratory tests reported in the literature indicate that the strength of a material (of given porosity) decreases when the flaw size increases. In DEM simulations, stress redistribution after bond breakage leads to another stable position of equilibrium. Therefore breakage does not propagate from one bond to the neighboring bonds. The total force needed to fragment a particle is the sum of the contact forces needed to break all the elementary bonds inside that particle. More sophisticated models are needed to capture unstable fracture propagation and consequent cluster strength variations in DEM [28]. This being said, our results confirm the strong dependence of particle strength to porosity, already noted in uniaxial compression strength (UCS) tests performed on porous rock samples [39] [40].

5. Conclusion

We modeled a crushable sand particle as a quasi-spherical cluster of bonded, hexagonally packed, equally sized, non-breakable balls. With this Distinct Element Model (DEM), a series of single-particle uniaxial compression tests were simulated by controlling the velocity of two rigid walls, placed at the top and bottom of the cluster. We calibrated the DEM parameters so as to match the displacement and axial force obtained experimentally at the first particle fragmentation. Then the calibrated cluster model was used to

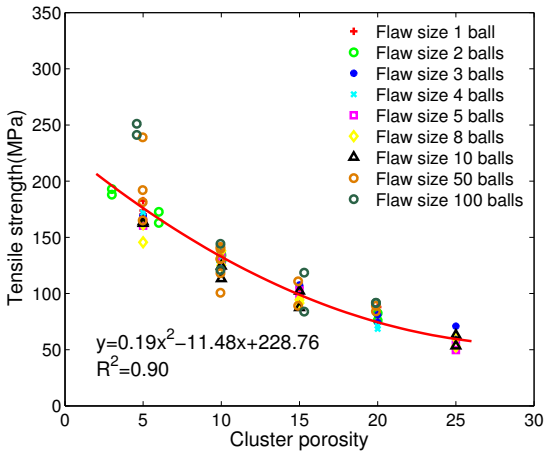

Figure 16: Effect of porosity on particle tensile strength.

simulate shielding and size effects at the particle scale. In order to study the influence of the coordination number on particle crushing, we modeled the mechanical confinement effect of neighboring particles by placing rigid walls around the cluster. We used symmetric distributions of walls for coordination numbers lower than 60, and both symmetric and random wall distributions for higher coordination numbers. We found that the axial force necessary to trigger the first fragmentation increases linearly with the coordination number. In order to understand why larger particles have lower tensile strength, we studied size effects on the crushing process of clusters with and without internal flaws. At constant flaw size and cluster porosity, we found that the cluster tensile strength did not depend on the cluster size as long as the ratio ball size / cluster size was smaller than 0.014 (i.e. for clusters that contained at least 37,000 elementary balls). We also verified that the tensile strength of a particle of given size decreases when, for a given flaw size (respectively for

a given number of flaws), the number of flaws increases (respectively the flaw size increases). For clusters with a porosity ranging between 0% and 30%, tensile strength only depends on porosity and not on flaw size. The results thus show that particle strength depends: (1) linearly on particle coordination number; (2) quadratically on particle porosity. The numerical methods presented in this paper will be improved to model the process of fragmentation within an assembly of particles and predict the combined actions of shielding and size effects. Theoretical and DEM modeling of particle crushing will advance the fundamental understanding of energy transfer in particulate media, which can be used to design infrastructure (e.g., ballast), shielding materials (e.g., packaging), food and medical products (e.g., tablets).

Acknowledgements

Support for this research was provided by the American Association of Railroads, as part of the project entitled "Modeling Ballast Particle Crushing as a Phase Change".

References Cited

[1] B. Aursudkij, A laboratory study of railway ballast behaviour under traffic loading and tamping maintenance, Ph.D. thesis, Nottingham Trent University (2007).

[2] P. V. Lade, J. A. Yamamuro, P. A. Bopp, Significance of particle crushing in granular materials, Journal of Geotechnical Engineering 122 (4) (1996) 309–316.

[3] I. Cavarretta, The influence of particle characteristics on the engineering behaviour of granular materials, Ph.D. thesis, Imperial College London London (2009).

[4] I. Cavarretta, C. O'SULLIVAN, The mechanics of rigid irregular particles subject to uniaxial compression, Géotechnique 62 (8) (2012) 681–692.

[5] B. Darvell, Uvniaxial compression tests and the validity of indirect tensile strength, Journal of Materials Science 25 (l990) (1990) 757–780.

[6] J. Jaeger, Failure of rocks under tensile conditions, in: International Journal of Rock Mechanics and Mining Sciences & Geomechanics Abstracts, Vol. 4, Elsevier, 1967, pp. 219–227.

[7] O. Tsoungui, D. Vallet, J.-C. Charmet, Numerical model of crushing of grains inside two-dimensional granular materials, Powder technology 105 (1) (1999) 190–198.

[8] W. Lim, G. McDowell, The importance of coordination number in using agglomerates to simulate crushable particles in the discrete element method, Géotechnique 57 (8) (2007) 701–705.

[9] L. Scholtès, F.-V. Donzé, A dem model for soft and hard rocks: Role of grain interlocking on strength, Journal of the Mechanics and Physics of Solids 61 (2) (2013) 352–369.

[10] L. Scholtès, F.-V. Donzé, M. Khanal, Scale effects on strength of geomaterials, case study: coal, Journal of the Mechanics and Physics of Solids 59 (5) (2011) 1131–1146.

[11] Z. P. Bažant, Size effect in blunt fracture: concrete, rock, metal, Journal of Engineering Mechanics.

[12] Z. P. Bazant, M. T. Kazemi, T. Hasegawa, J. Mazars, Size effect in brazilian split-cylinder tests: measurements and fracture analysis, ACI Materials Journal 88 (3) (1991) 325–332.

[13] W. L. Lim, Mechanics of railway ballast behaviour, Ph.D. thesis, University of Nottingham (2004).

[14] A. A. Griffith, The phenomena of rupture and flow in solids, Philosophical transactions of the royal society of london. Series A, containing papers of a mathematical or physical character (1921) 163–198.

[15] Y. Hiramatsu, Y. Oka, Determination of the tensile strength of rock by a compression test of an irregular test piece, in: International Journal of Rock Mechanics and Mining Sciences & Geomechanics Abstracts, Vol. 3, Elsevier, 1966, pp. 89–90.

[16] D.-M. Lee, The angles of friction of granular fills., Ph.D. thesis, University of Cambridge (1992).

[17] W. Weibull, A statistical theory of the strength of materials, no. 151, Generalstabens litografiska anstalts förlag, 1939.

[18] G. McDowell, M. Bolton, On the micromechanics of crushable aggregates, Geotechnique 48 (5) (1998) 667–679.

[19] C. Ovalle, E. Frossard, C. Dano, W. Hu, S. Maiolino, P.-Y. Hicher, The effect of size on the strength of coarse rock aggregates and large

rockfill samples through experimental data, Acta Mechanica 225 (8) (2014) 2199–2216.

[20] S. Lobo-Guerrero, L. E. Vallejo, Application of weibull statistics to the tensile strength of rock aggregates, Journal of geotechnical and geoenvironmental engineering 132 (6) (2006) 786–790.

[21] P. A. Cundall, O. D. Strack, A discrete numerical model for granular assemblies, Geotechnique 29 (1) (1979) 47–65.

[22] Itasca, Particle Flow Code in Two Dimensions, Version 4.0., Itasca Consulting Group, Inc., Minnesota.

[23] M. B. Cil, K. A. Alshibli, 3d modeling of sand particle fracture using discrete element method and synchrotron micro-tomography images, in: Geo-Congress 2014 Technical Papers@ sGeo-characterization and Modeling for Sustainability, ASCE, 2014, pp. 2822–2829.

[24] Y. Cheng, Y. Nakata, M. Bolton, Discrete element simulation of crushable soil, Geotechnique 53 (7) (2003) 633–641.

[25] D. Robertson, Numerical simulations of crushable aggregates, Ph.D. thesis, Ph. D. dissertation, University of Cambridge (2000).

[26] G. McDowell, O. Harireche, Discrete element modelling of soil particle fracture, Géotechnique 52 (2) (2002) 131–135.

[27] K. L. Johnson, K. L. Johnson, Contact mechanics, Cambridge university press, 1987.

[28] N. a. Cho, C. Martin, D. Sego, A clumped particle model for rock, International Journal of Rock Mechanics and Mining Sciences 44 (7) (2007) 997–1010.

[29] J. F. Hazzard, R. P. Young, S. Maxwell, Micromechanical modeling of cracking and failure in brittle rocks, Journal of Geophysical Research: Solid Earth (1978–2012) 105 (B7) (2000) 16683–16697.

[30] E. Buckingham, On physically similar systems; illustrations of the use of dimensional equations, Physical Review 4 (4) (1914) 345–376.

[31] H. Huang, Discrete element modeling of tool-rock interaction, university of minnesota (1999).

[32] B. Yang, Y. Jiao, S. Lei, A study on the effects of microparameters on macroproperties for specimens created by bonded particles, Engineering Computations 23 (6) (2006) 607–631.

[33] S. Lei, P. Kaitkay, X. Shen, Simulation of rock cutting using distinct element method-pfc 2d, Numerical modeling in micromechanics via particle methods 1 (4) (2004) 63–72.

[34] D. Potyondy, P. Cundall, A bonded-particle model for rock, International journal of rock mechanics and mining sciences 41 (8) (2004) 1329–1364.

[35] A. Standard, D2487 (2011) standard practice for classification of soils for engineering purposes (unified soil classification system), ASTM International, West Conshohocken, PA www.ASTM.org.

[36] G. Marsaglia, et al., Choosing a point from the surface of a sphere, The Annals of Mathematical Statistics 43 (2) (1972) 645–646.

[37] S. Antonyuk, J. Tomas, S. Heinrich, L. Mörl, Breakage behaviour of spherical granulates by compression, Chemical engineering science 60 (14) (2005) 4031–4044.

[38] J. Billam, Some aspects of the behaviour of granular materials at high pressure, stress-strain behaviour of soils.

[39] M. P. Schöpfer, S. Abe, C. Childs, J. J. Walsh, The impact of porosity and crack density on the elasticity, strength and friction of cohesive granular materials: insights from dem modelling, International Journal of Rock Mechanics and Mining Sciences 46 (2) (2009) 250–261.

[40] C. Chang, M. D. Zoback, A. Khaksar, Empirical relations between rock strength and physical properties in sedimentary rocks, Journal of Petroleum Science and Engineering 51 (3) (2006) 223–237.